

Sisyphus Effect in Pulse Coupled Excitatory Neural Networks with Spike-Timing Dependent Plasticity

Kaare Mikkelsen,¹ Alberto Imparato,¹ and Alessandro Torcini^{2,3,1}

¹*Dept. of Physics and Astronomy, University of Aarhus,
Ny Munkegade, Building 1520 - DK-8000 Aarhus C, Denmark*

²*CNR - Consiglio Nazionale delle Ricerche - Istituto dei Sistemi Complessi,
via Madonna del Piano 10, I-50019 Sesto Fiorentino, Italy*

³*INFN Sez. Firenze, via Sansone, 1 - I-50019 Sesto Fiorentino, Italy*

(Dated: May 17, 2018)

The collective dynamics of excitatory pulse coupled neural networks with spike timing dependent plasticity (STDP) is studied. Depending on the model parameters stationary states characterized by High or Low Synchronization can be observed. In particular, at the transition between these two regimes, persistent irregular low frequency oscillations between strongly and weakly synchronized states are observable, which can be identified as infraslow oscillations with frequencies $\simeq 0.02 - 0.03$ Hz. Their emergence can be explained in terms of the Sisyphus Effect, a mechanism caused by a continuous feedback between the evolution of the coherent population activity and of the average synaptic weight. Due to this effect, the synaptic weights have oscillating equilibrium values, which prevents the neuronal population from relaxing into a stationary macroscopic state.

PACS numbers: 05.45.-a,05.45.Jn,87.19.lj,05.45.Xt

I. INTRODUCTION

Fluctuating spontaneous neural activity has been observed in several areas of the brain: ranging from the cortex to the hippocampus, from the thalamus to the basal ganglia and cerebellum [1, 2]. In particular, low-frequency fluctuations (LFFs), in the range 0.5-1 Hz, have been observed in the cortical local field potential (LFP) during sleep as well as during quiet wakefulness [3, 4]. In the hippocampus, this kind of irregular oscillations between states, characterized by higher and lower levels of synchrony, have been revealed during slow-wave sleep and related to the process of memory consolidation in the neocortex [5]. Infraslow oscillations (ISOs), corresponding to frequencies $\simeq 0.02 - 0.2$ Hz, have been identified in humans using high-density fullband electroencephalography during the execution of somatosensory detection tasks and during sleep [2, 6, 7]. Furthermore, these infraslow oscillations have been associated to a cyclic modulation of cortical excitability, possibly related to the aggravation of epileptic activity during sleep [7].

Synaptic plasticity is a fundamental ingredient of neuronal activity, being involved in the transfer of information and in its processing at the neuronal and population level. On the one hand, during the sleep-wake cycle, distinct oscillatory patterns organize the activity of neuronal populations, modulating synaptic plasticity [8]. On the other hand, synaptic plasticity has been identified as one of the fundamental mechanisms at the origin of multistable states in neural circuits [9–13]. In particular, spike-timing dependent plasticity (STDP) represents an important, experimentally measured, mechanisms controlling the strength of the synapse connecting a pre-synaptic to a post-synaptic neuron. STDP is a temporally asymmetric form of Hebbian learning, based on the causal relationship between the spikes emitted at pre- and postsynaptic neurons [14–19]. A spike emitted in the pre-synaptic cell, within a certain time interval (learning window), before an emission in the postsynaptic cell triggers long-term potentiation (LTP), whereas the reversed temporal order in spike emission results in long-term depression (LTD) [20]. Learning windows for LTD and LTP are asymmetric, as clearly shown experimentally [21–23].

It has been shown, both experimentally [24] and theoretically [25, 26], that STDP influences the collective behavior of a neural population, generally leading to an increase in the degree of synchronization. However, in the presence of propagation delays STDP can instead provide a negative feedback mechanism contrasting highly synchronized network activity [11]. The presence of noise in this latter case can lead to the emergence of states at the boundary between randomness and synchrony, while in oscillatory neural networks the desynchronizing effect due to noise is counteracted by the STDP action [27–29]. On a general ground the asymmetry in the learning windows seems a prerequisite for the emergence of coexisting states with different degree of synchronization [9, 10, 30].

In this paper, we study the *Sisyphus Effect* (SE), a deterministic mechanism recently introduced to explain the spontaneous emergence of irregular oscillations in the neural population activity in presence of STDP [31]. In particular, we include STDP in the renowned neural network model developed in [32] by Abbott and van Vreeswijk. This model is composed of leaky integrate-and-fire (LIF) neurons and the synaptic interactions are purely excitatory and mediated by α -pulses [33]. In absence of plasticity, the network activity is asynchronous for slow synapses (and/or

large synaptic weights) and partially synchronized for sufficiently fast synapses (and/or weak coupling) [34–36]. Similar to Sisyphus, who was bound in Tartarus for the eternity to roll a boulder uphill just to watch it rolling back down again, STDP leads the asynchronous system towards a synchronized state by modifying the synaptic weights, however as soon as the synchronous regime is achieved the weights are attracted back towards their starting values and the system desynchronizes. Thus STDP should repeat its action again and again, and this leads to endless oscillations in the synchronization level of the population activity.

The paper is organized as follows, Sect. II is devoted to the introduction of the model, of the integration scheme as well as of the indicators employed to characterize the degree of synchronization of the neural population and its collective activity. The collective dynamics in plastic and non-plastic neural networks is described in Sect. III with particular emphasis on the emergence of LFFs. Sect. IV reports a characterization of the synchronization oscillations in the neural activity in terms of the evolution of an order parameter on an effective free energy landscape. The results of simulations, performed by maintaining a constant average synaptic weight, are analyzed in Sect. V, while Sect. VI is devoted to the mean-field analysis of the synaptic weights evolution. The SE is illustrated in Sect. VII for different synaptic parameters. Finally a brief summary and a synthetic discussion of the reported results can be found in Sect. VIII. In Appendix A the stationary distributions of the synaptic weights are displayed for different parameters, while Appendix B reports the transformations required to convert the variables and parameters entering in the model from adimensional units to physical ones.

II. MODEL AND INDICATORS

A. Neural Network Model

We study a fully coupled network composed of N Leaky Integrate-and-Fire (LIF) neurons, whose membrane potentials $V_i(t) \in [V_r : V_{th}]$ are ruled by the following equation:

$$\dot{V}_i(t) = a - V_i(t) + I_i(t) \quad i = 1, \dots, N \quad ; \quad (1)$$

where I_i is the synaptic current due to the inputs received from the rest of the network, a is the intrinsic excitability of the neuron which can be due to nonspecific background currents arising from distant brain areas or to external DC current terms, in particular we assume that the neuron is suprathreshold, i.e. $a > 1$. Whenever the neuron i reaches the threshold $V_{th} \equiv 1$, a pulse $p_\alpha(t)$ is instantaneously transmitted to all the other neurons and its membrane potential is reset to $V_r \equiv 0$. The synaptic current can be written as $I_i(t) = gE_i(t)$, with $g > 0$ representing the excitatory *homogeneous* synaptic strength, while the field $E_i(t)$ is given by the linear superposition of all the pulses $p_\alpha(t)$ received by neuron i in the past. The formal expression of $E_i(t)$ reads as

$$E_i(t) = \frac{1}{N-1} \sum_{n|t_n < t} w_{ij}(t_n) \Theta(t - t_n) p_\alpha(t - t_n) \quad , \quad (2)$$

where $N - 1$ is the number of pre-synaptic neurons, since autapses have been avoided, $\Theta(t)$ is the Heaviside function and w_{ij} represents the synaptic weight associated to a directional link connecting the pre-synaptic neuron j to the post-synaptic one i at the time of spike emission, t_n . The scaling of the field E_i with the number of synaptic inputs reported in (2) is intended to mimic the homeostatic synaptic scaling experimentally observed for excitatory neurons [37].

Following van Vreeswijk [36], we assume α -function shape for the pulses, i.e. $p_\alpha(t) = \alpha^2 t \exp(-\alpha t)$. The time evolution of the field $E_i(t)$ is thus ruled by the following second order differential equation:

$$\ddot{E}_i(t) + 2\alpha\dot{E}_i(t) + \alpha^2 E_i(t) = \frac{\alpha^2}{N-1} \sum_{n|t_n < t} w_{ij}(t_n) \delta(t - t_n) \quad . \quad (3)$$

For a fully coupled network, in absence of plasticity, the weights w_{ij} appearing in Eq. (2) and (3) are all equal to one (apart from the autaptic terms which are set to zero) and the fields E_i are all identical, therefore the neurons are driven by a common field E . In presence of plasticity we assume that the synaptic weights evolve in time according to the STDP rule with soft bounds, namely

$$\dot{w}_{ij}(t) = p[w_{max} - w_{ij}(t)]A_j S_i - d w_{ij}(t) B_i S_j \quad , \quad (4)$$

where d (p) is the potentiation (depression) amplitude, and $S_k = \sum_{n|t_n < t} \delta(t - t_n)$ represents the time series of spikes emitted by neuron k until time t . The presence of the bound implies that $0 \leq w_{ij} \leq w_{max}$.

The variables A_j can be thought of as concentrations of glutamate bound to the post-synaptic receptors, or as the fraction of open N-methyl-D-aspartate (NMDA) receptors; while B_i it is usually associated to the concentration of calcium entering the cell due to a back-propagating action potential [20].

In particular, we have implemented the *nearest neighbor* version of the STDP rule [20, 27], where the synapses have memory just of the last emitted spike. In this case the time evolution of the A_j and B_i variables is given by

$$\tau_+ \dot{A}_j = -A_j + (1 - A_j)S_j \quad , \quad \tau_- \dot{B}_i = -B_i + (1 - B_i)S_i \quad , \quad (5)$$

where τ_+ (τ_-) are the time scales at which post- (pre-) synaptic spikes will cause potentiation (depression) of the synapse. As pointed out by Izhikevich and Desai [38] the nearest neighbor implementation of the STDP rule is consistent with the classical long-term potentiation and depression as represented in the form of the Bienenstock-Cooper-Munro synapse [39].

Therefore, in the case of a post-synaptic (pre-synaptic) spike, emitted by neuron i (j) at time t , the weight w_{ij} is potentiated (depressed) as

$$w_{ij}(t^+) = w_{ij}(t^-) + \Gamma_{ij}(t) \quad (6)$$

with

$$\Gamma_{ij}(t) = \begin{cases} p[w_M - w_{ij}(t^-)]e^{-\frac{\delta_{ij}}{\tau_+}} & \text{if } \delta_{ij} > 0 \\ -d w_{ij}(t^-)e^{+\frac{\delta_{ij}}{\tau_-}} & \text{if } \delta_{ij} < 0 \end{cases} \quad (7)$$

where $\delta_{ij} = t - t^{(j)} > 0$ ($\delta_{ij} = t^{(i)} - t < 0$) is the firing time difference and $t^{(k)}$ the last firing time of neuron k . The resulting distributions of the synaptic weights and their properties of stationarity are discussed in the Appendix A.

In this paper, we assume that $\tau_- > \tau_+$, as suggested by the experimental data [15, 23], and in particular we fix $\tau_- = 3\tau_+ = 0.3$. Furthermore, despite that the main part of the reported results refer to $d = p = 0.01$ (*Symmetric Case*, SC), we have also examined a more realistic situation where $p > d$ (as suggested by the experiments reported in [15, 23]), namely by considering $p = 2d = 0.02$ (*Asymmetric Case*, AC). If not explicitly stated the SC will be studied for $\alpha = 9$ and the AC for $\alpha = 11$. The studied model is adimensional, however it can easily be transformed to physical units as shown in Appendix B.

B. Simulation Method

Since the plasticity rule depends critically on the precision of the spiking events, it is necessary to employ an accurate integration scheme to update the evolution equations. This makes an event-driven algorithm an optimal choice, because it conjugates high accuracy in the determination of the spike times with a fast implementation [28]. In particular, by following Olmi et al. [40] the event-driven map can be written as

$$\begin{aligned} E_i(n+1) &= E_i(n)e^{-\alpha\tau(n)} + P_i(n)\tau(n)e^{-\alpha\tau(n)} \\ P_i(n+1) &= P_i(n)e^{-\alpha\tau(n)} + w_{im}\frac{\alpha^2}{N-1} \\ V_i(n+1) &= V_i(n)e^{-\tau(n)} + a(1 - e^{-\tau(n)}) + gH_i(n) \quad i = 1, \dots, N \quad ; \quad V_m(n+1) \equiv 0; \end{aligned} \quad (8)$$

where $P_i \equiv \alpha E_i + \dot{E}_i$ is an auxiliary variable, m is the index of the neuron emitting the $n+1$ -th spike and $\tau(n) = t_{n+1} - t_n$ is the network inter-spike interval. The explicit expression for the nonlinear function $H_i(n)$ appearing in (9) is

$$H_i(n) = \frac{e^{-\tau(n)} - e^{-\alpha\tau(n)}}{\alpha - 1} \left(E_i(n) + \frac{P_i(n)}{\alpha - 1} \right) - \frac{\tau(n)e^{-\alpha\tau(n)}}{(\alpha - 1)} P_i(n); \quad (9)$$

for the parameter values considered in this paper ($g > 0$ and $a > 1$), $H_i(n) > 0$.

The event driven map reported in (9) gives the explicit evolution of the fields E_i, P_i and membrane potentials V_i from the time t_n^+ immediately following the n -th spike emission to time t_{n+1} . However, the evolution equation depends on the inter-spike interval $\tau(n)$, which can be determined only implicitly by solving the following equation

$$\tau(n) = \ln \left[\frac{a - V_m(n)}{a + gH_m(n) - 1} \right]. \quad (10)$$

Together with the evolution of the fields and membrane potentials, also the weights of the afferent and efferent synapses associated to the firing neuron m should be updated as follows

$$\begin{aligned} w_{mj}(n+1) &= w_{mj}(n) + p[w_{max} - w_{mj}(n)]e^{-\Delta t_j/\tau_+} \\ w_{jm}(n+1) &= w_{jm}(n) - dw_{jm}(n)e^{-\Delta t_j/\tau_-} \quad j = 1, \dots, N \quad w_{jj} \equiv 0 \end{aligned} \quad (11)$$

where $\Delta t_j = t_{n+1} - t^{(j)}$ and $t^{(j)}$ is the last firing time of neuron j . Please notice that the synapses evolution (11) is performed after the map evolution (9), because we assume that the plasticity is a slower process than spike generation.

The implementation of the event driven map (9) involves $3N - 1$ variables, since the membrane potential of the firing neuron is exactly zero at each firing event, thus it does not take part in the dynamics. The evolution of the synaptic weights involves $N^2 - N$ variables, since autapses have been excluded. Altogether our dynamical systems has $N^2 + 2N - 1$ degrees of freedom. Our implementation of the dynamical evolution of the network assumes that only one neuron at a time will reach the threshold, therefore in the case of exact clustering, without any source of disorder, our method will fail. However, we have always verified our assumption to be true.

In the following we report two kinds of simulations: *Constrained* (CS) and *Unconstrained* (US). The results of CSs are discussed in Sect. V, during CSs the synaptic weights are constrained to have an average value

$$W(t) \equiv \frac{1}{N(N-1)} \sum_{i,j} w_{ij}(t) \quad , \quad (12)$$

which remains equal to W_0 . To achieve this result the weights w_{ij} are let to evolve following their dynamics, as expressed in Eqs. (11), however at regular time intervals the weights are rescaled as $w_{ij}/W(t) \cdot W_0$ in order to maintain their average value constant ¹

C. Synchronization Indicator and Local Field Potential

The degree of synchronization of the neuronal population can be characterized in terms of the order parameter [41, 42]

$$R(t) = \left| \frac{1}{N} \sum_k e^{i\theta_k(t)} \right| \quad , \quad (13)$$

where

$$\theta_k(t) = 2\pi \frac{(t - t_m^{(k)})}{(t_{m+1}^{(k)} - t_m^{(k)})} \quad (14)$$

is the phase of the k -th neuron at time t between its m -th and $(m+1)$ -th spike emission, occurring at times $t_m^{(k)}$ and $t_{m+1}^{(k)}$, respectively. A non-zero R value is an indication of partial synchronization, perfect synchronization is achieved for $R = 1$, while a vanishingly small $R \sim 1/\sqrt{N}$ is observable for asynchronous states in finite systems.

To better reveal the dynamics on long time scales, we have low-pass filtered $R(t)$ by performing the following convolution integral

$$R_f(t) = \frac{1}{\tau_F} \int_0^{T_M} R(t - \xi) e^{-\xi/\tau_F} \quad , \quad (15)$$

where τ_F^{-1} represents the cut-off frequency, and $T_M \gg \tau_F$ is the integration window.

The local field potential (LFP) can be defined by following [43–45] as

$$LFP(t) \equiv -I_f(t) = \frac{1}{\tau_F} \int_0^{T_M} \frac{1}{N} \sum_{i=1}^N I_i(t - \xi) e^{-\xi/\tau_F} \quad , \quad (16)$$

¹ For $N = 200$ we renormalized the synaptic weights each 0.2 time units to avoid drifts in the synaptic average value. All the other results discussed in the article refer to USs, where no constraint was imposed on the dynamics.

where $I_f(t)$ represents the filtered input synaptic current averaged over the ensemble of all neurons. We can consider $LFP(t)$ as the local field potential generated by our ensemble of neurons if they would be all located at the same spatial distance from the recording electrode, the low-pass filtering action of dendrites and of the extracellular medium are taken into account by performing the convolution integral reported in (16) [46]. To compare with experimental measurements where high (low) activity correspond to a minimum (maximum) in the LFP, we reversed the sign of the filtered synaptic current in (16) [1]. In the following, we have usually employed $\tau_F = 40$ and $T_M = 300$ and we considered $R(t)$ and $I_i(t)$ sampled at equal time intervals $\delta T = 1$.

III. NON PLASTIC VERSUS PLASTIC COLLECTIVE DYNAMICS

In this Section we compare the possible collective dynamics observable at the macroscopic level in the non plastic and plastic networks by characterizing the different macroscopic attractors in terms of their degree of synchronization, described by R .

A. Non plastic network

In absence of plasticity the dynamics of the model is controlled by three parameters: namely, the neuronal intrinsic excitability a , the synaptic strength g and the inverse pulse width α . As shown in Fig. 1, where the phase diagrams in the plane (g, a) and (g, α) are reported, only two collective behaviors can be observed for the non plastic fully connected network: an asynchronous and a partially synchronous regime.

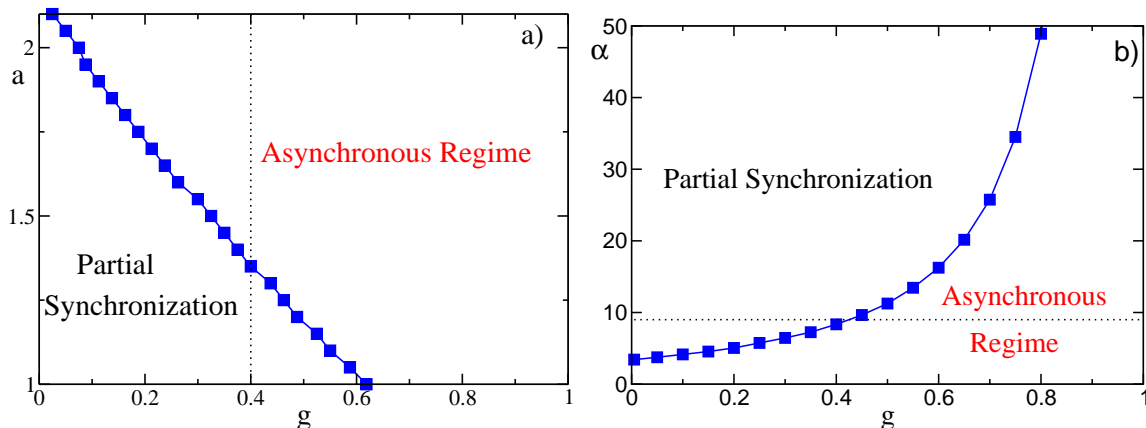


FIG. 1: (color online) Phase diagram for the homogeneous model without plasticity, in (a) we report the phase plane (g, a) , while in (b) the phases are shown in the (g, α) -plane. The blue filled squares indicate the critical values for which the asynchronous state (namely, the splay state) becomes unstable; the dotted line indicates $g = 0.4$ in (a) and $\alpha = 9$ in (b). The other parameters are fixed to $\alpha = 9$ in (a) and $a = 1.3$ in (b) and the system size is $N = 100$.

In this case the asynchronous regime corresponds to a so-called *splay state* [32, 47]: this is an exact solution for the system which is perfectly asynchronous ($R \equiv 0$). Furthermore, this solution is characterized by a constant field E (where the neuron dependence has been dropped since in this case the fields are all identical) and a periodic evolution of the membrane potentials. For this solution we are able to perform an exact analytic linear stability analysis [47], and therefore to determine the stability boundaries of the solution, reported as solid line plus symbols in Fig. 1. It is known that whenever the splay state loses its stability it gives rise to a partially synchronized regime via a Hopf supercritical bifurcation [32]. This regime is characterized, beside a finite value of R , by a periodically oscillating macroscopic field E and by a quasi-periodic motion of the membrane potentials at a microscopic level. This regime has been mainly observed in pulse coupled neural networks [36], but recently partial synchronization has been discovered also in networks of phase oscillators [48, 49]. and electronic Wien-bridge devices [50] coupled via mean-field nonlinear coupling. In this state the single neuron dynamics are quasi-periodic and the field E periodic with a period which is incommensurate with respect to the single neuron inter-spike interval (ISI) [51].

The transition may be intuitively understood as an interplay between the two time scales present in the model: the ISI and the pulse width $1/\alpha$. We observe from Fig. 1 (a) and (b) that the asynchronous regime is stable for small

α -values and for large a - and g -values. The intrinsic excitability and the (excitatory) synaptic coupling determines the ISI, in particular, the ISI duration is a decreasing function of the values of a and g . At sufficiently low α , the synaptic current seen by each neuron is essentially constant, and it induces a stable regular network activity corresponding to a periodic firing of successive neurons with a constant population spiking rate. Whenever the pulse duration drops below a certain value the synaptic input cannot be anymore regarded as constant and the state corresponding to a time-invariant network activity becomes unstable. For α -values very large with respect to the ISI, an “almost” fully synchronized state with $R \simeq 1$ is observed, as expected for excitatory networks where the transmitted pulses have extremely short rise times, like exponential or δ -spikes [34, 35, 52]. With reference to the parameter values considered in this paper, partial synchronization emerges for $a \leq a_c \simeq 1.35$ for fixed coupling $g = 0.4$, and for $g \leq g_c \simeq 0.4676$ for fixed pulse width $\alpha = 9$, see Fig. 1.

In order to characterize the network dynamics it is tempting to introduce an unique parameter encompassing the two time scales, similarly to what was done in [47] to analyze the linear stability of the splay state. This adimensional parameter is the ratio of the two relevant time scales, namely

$$Q = \frac{\langle ISI \rangle}{1/\alpha} = \alpha \langle ISI \rangle \quad ; \quad (17)$$

where $\langle \cdot \rangle$ denotes an average over the neuronal population and over the sequence of spikes. In Fig. 2 (a) we report the average level of synchronization \bar{R} for a large variety of states corresponding to different (a, g, α) -triples as a function of Q : as one can notice the data almost collapse onto a universal curve. This indicates that, to a certain extent, the non plastic network three-dimensional phase space (a, g, α) can be described by the single parameter Q . Furthermore, we observe states with $\bar{R} = 0$ for low Q values, namely smaller than $Q \simeq 8.15$, while a partially synchronized state is observable at large $Q > 6$. Therefore there is a limited interval $Q \simeq 6 - 8$, where to the same Q value can correspond either asynchronous or partially synchronized states. However this does not necessarily imply a coexistence of the possible attractors, but simply that the parametrization of the dynamical behaviors in terms of an unique parameter Q is not perfect.

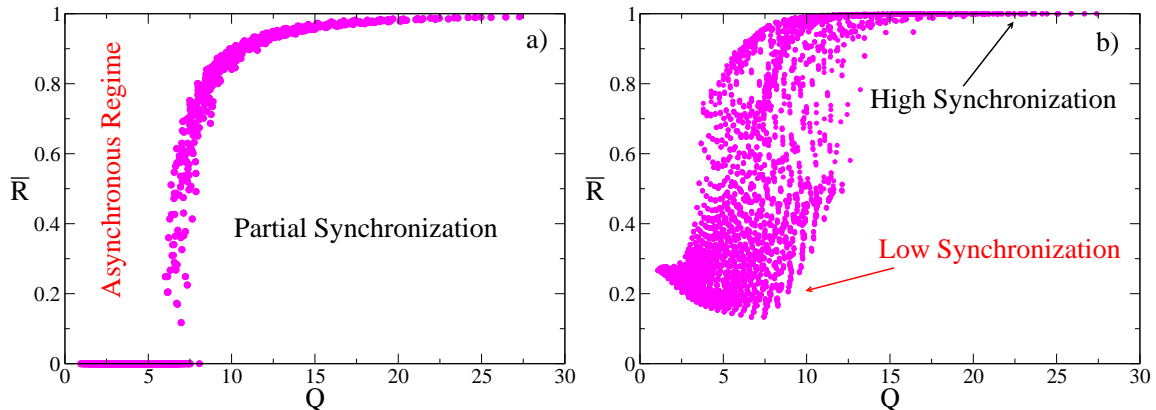


FIG. 2: (color online) Time averaged \bar{R} as a function of Q : (a) non plastic network; (b) plastic network with $p = d = 0.01$, $\tau_- = 3\tau_+ = 0.3$. Each plot consists of 1,575 different sets of parameters (a, g, α) , with $1.1 \leq a \leq 2.5$, $0.1 \leq g \leq 0.9$, $8 \leq \alpha \leq 12$, $N = 300$. In the non plastic (plastic) case each set of parameters have been simulated for 2 (4) different initial conditions and the average performed over a time span of 10^5 time units. The measured differences among the various realizations are smaller than the dimension of the dots.

B. Plastic network

Upon the addition of STDP, the data do not collapse anymore onto a universal curve, as we would expect since new time scales now enter in the model microscopic dynamics: namely, the learning time windows. The data reported in Fig. 2 (b) indicate that at large $Q > 15$ the presence of plasticity essentially does not modify the collective behavior already observed in the non plastic network: the system remains almost fully synchronized $\bar{R} \simeq 1$ (*High Synchronization* (HS)). However, the introduction of plasticity influence the dynamical evolution at smaller Q , for $Q < 2$ the completely asynchronous state disappears and it is substituted by a regime of *Low Synchronization* (LS), where $\bar{R} \simeq 0.3$. Furthermore, in the intermediate Q range the neuronal population exhibits a large variability in the

level of synchronization, as measured by the \bar{R} parameter and this regime will be the main subject of our investigation. All in all these results suggest that the introduction of STDP favors synchronization in the system.

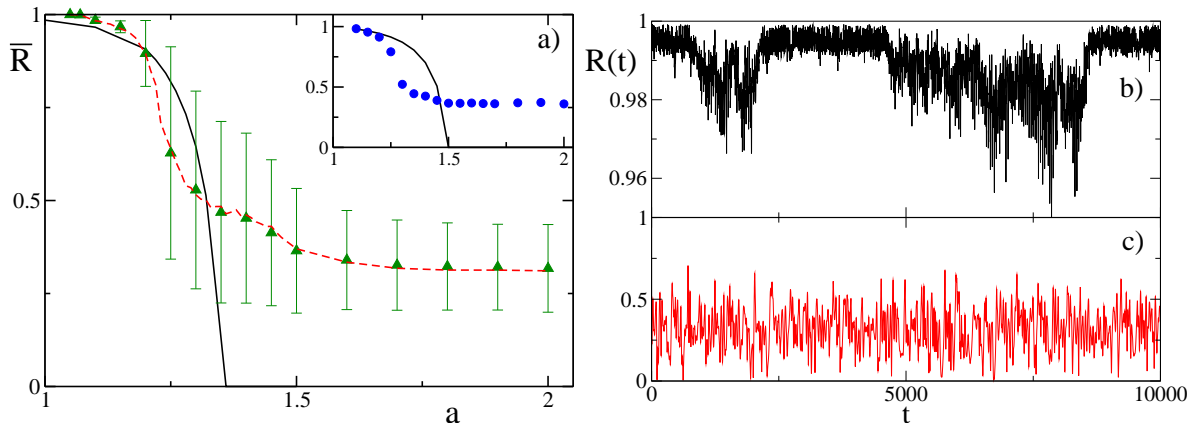


FIG. 3: (color online) (a) Average order parameter \bar{R} as a function of the intrinsic excitability a for the nonplastic network (black solid line) and in the presence of STDP for the SC, namely $\alpha = 9$ and $d = p = 0.01$ (the green triangles refer to $N = 200$ and the red dashed line to $N = 500$). The inset reports the data for $\alpha = 11$ and $N = 300$ for the non plastic network (black solid curve) and with STDP for the AC with $p = 2d = 0.02$ (blue dots ●). (b) and (c) Time evolution of $R(t)$ for the SC with $N = 500$ for $a = 1.09$ and $a = 1.70$, respectively. The data refer to $g = 0.4$, $\tau_- = 3\tau_+ = 0.3$ and $w_{max} = 2$ and the averages have been performed over a time span $\simeq 10^4$, after discarding a transient $\simeq 10^5$.

In particular, we will focus on the dependence of the macroscopic dynamics on the intrinsic excitability a . The time averaged order parameter \bar{R} is reported as a function of a in Fig. 3 (a) for the non plastic situation as well as for the plastic case.

As already stressed, the introduction of STDP destabilizes the asynchronous state that is now substituted by a Low Synchronization state with $\bar{R} \simeq 0.32 - 0.35$ for the set of parameters considered in the figure. Furthermore, at low excitability $a \simeq 1 - 1.2$ the systems is almost fully synchronized $\bar{R} \simeq 1$, but the macroscopic evolution reveals *high frequency fluctuations* (HFFs) (see Fig. 3 (b)). For high excitability $a \geq 1.5$ $R(t)$ oscillates quite rapidly around a finite non zero value as shown in Fig. 3 (c). The most part of the reported results refer to equal potentiation and depression amplitudes (SC), however these findings are essentially confirmed also for the more realistic AC, as shown in the inset of Fig. 3 (a).

To better characterize the regimes observable in the SC, we have estimated the power spectra S_R associated to $R(t)$ reported in Fig. 4, the spectrum for $a = 1.1$ resembles a Lorentzian with subsidiary peaks at low periods (namely $T < 35$). The Lorentzian part of the spectrum can be fitted as $\simeq 1/(\lambda^2 + T^{-2})$, thus indicating that it originates from a Poissonian point process with a relaxation time $\lambda^{-1} \simeq 1,400 - 2,000$. Furthermore, the S_R corresponding to $a = 1.9$ reveals two nearby HFF peaks at $T \simeq 70$ and 150.

However, the most interesting dynamical behavior can be observed for intermediate values of the intrinsic excitability, namely we will focus on $a = 1.3$. As shown in Fig. 5, for this value of the excitability the order parameter R widely fluctuates in time from $R \simeq 0$ to $R \simeq 1$, thus indicating that the system jumps irregularly between desynchronized and highly synchronized phases. This behavior is also observable for the AC as shown in Fig. 5 (b). The evolution of R reveals *Low Frequency Fluctuations* (LFFs) on time scales of the order of $1,300 \pm 400$ for the SC ($\simeq 700$ for the AC, data not shown), as it can be clearly appreciated by the corresponding power spectrum reported in Fig. 6 (a). In addition S_R exhibits also a small subsidiary peak at $T \simeq 50 - 60$ for the SC ($\simeq 45$ for the AC) indicating that the HFFs are still present. It is remarkable that low frequency oscillations are associated to the relaxation period $\simeq \lambda^{-1}$ previously identified for $a = 1.1$. This seems to suggest that by increasing the neuronal excitability the relaxation process becomes an oscillatory one. Somehow the increased excitability is now capable to sustain slow collective oscillations, which however for larger a disappears (as shown in Fig. 4 (b)). Furthermore, the LFFs for to the AC occurs definitely on a faster time scale.

Let us now estimate the physical time scales over which the observed LFFs take place, by assuming a membrane time constant $\tau \simeq 30 - 40$ ms (see Appendix B for the conversion units), the frequencies of the slow oscillations are $\simeq 0.02 - 0.03$ Hz therefore they correspond to infraslow rhythms as reported in Ref. [6]. On the other hand, the observed HFFs occur in a range of frequencies at the border between slow and infraslow waves, namely $0.16 - 1$ Hz [2].

To better characterize this regime we report in Fig. 5 also the time evolution of the average synaptic weight $W(t)$, as defined in Eq. (12). This quantity also reveals low frequency oscillations similar to those of $R(t)$, but occurring with some time delay. This suggests that $W(t)$ is somehow following the dynamics of $R(t)$, but the absence of HFFs

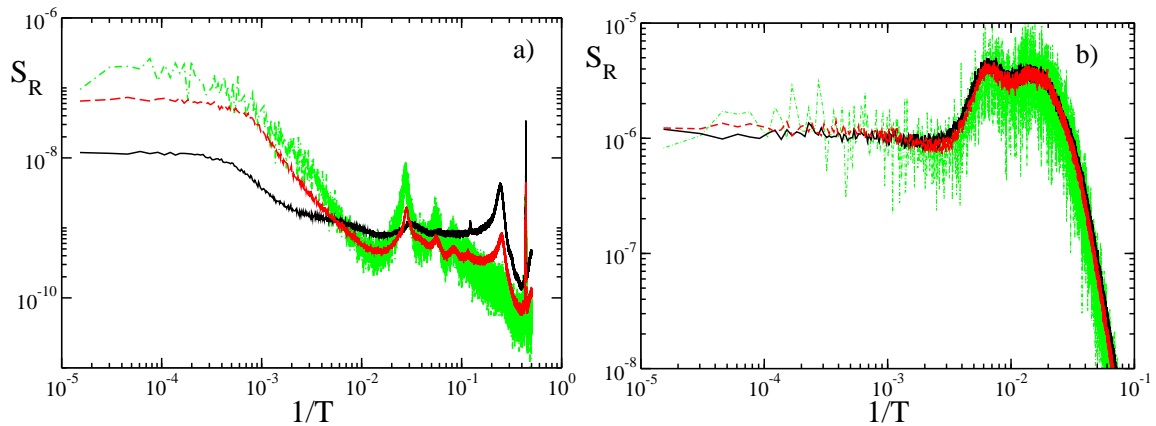


FIG. 4: (color online) Power spectra of the order parameter for different excitability, namely $a = 1.10$ (a) and $a = 1.90$ (b). The (black) solid line refers to $N = 100$, the (red) dashed to $N = 200$ and the (green) dot-dashed to $N = 400$ neurons. The data refer to SC for $g = 0.4$, $\alpha = 9$, $d = p = 0.01$, $\tau_- = 3\tau_+ = 0.3$ and $w_{max} = 2$ and are obtained after discarding a transient $\simeq 10^5$. The power spectra have been obtained by the time trace of the parameter R sampled at regular intervals $\delta T = 1$ and for a time window $T_{tot} = 65,536$, the spectra are averaged over 300-600 different time windows at $N = 100$ and 200 over 5-10 windows for $N = 400$.

in the dynamics of $W(t)$ reveals that the average synaptic weight reveals a sort of *inertia*, since it does not respond on short time scales to the modifications of the level of synchronization in the network.

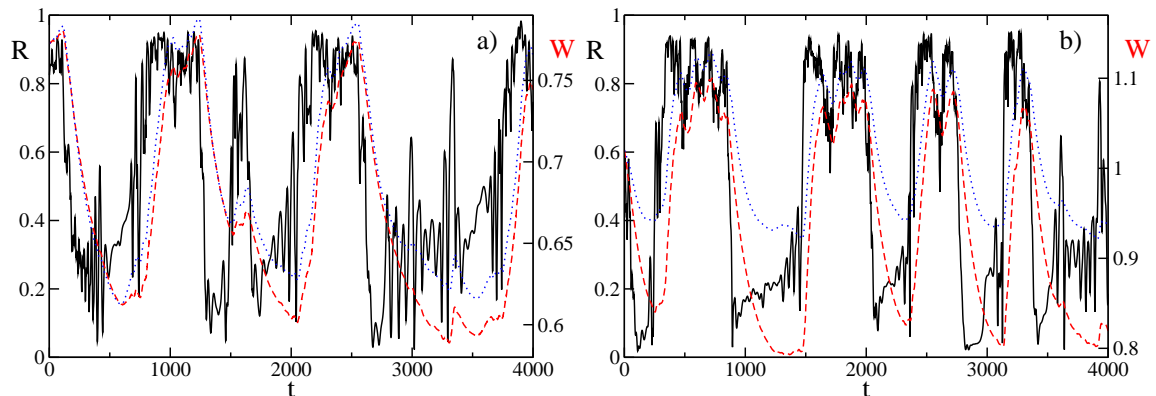


FIG. 5: (color online) Time evolution of R (black solid line) and of W (red dashed line) for $N = 2000$ neurons. The dotted (blue) line is the mean-field prediction obtained by employing the map $W(t + \Delta t) = W(t) + \Gamma(t)$, with Γ given by Eq. 18. The data refer to $a = 1.3$, $g = 0.4$, $d = 0.01$; (a) $p = 0.01$, $\alpha = 9$; (b) $p = 0.02$, $\alpha = 11$ and are measured after a transient $\simeq 10^4$. The mean-field predictions have been evaluated with $\Delta t = 1$, tests performed with $0.5 \leq \Delta t \leq 40$ did not lead to any peculiar difference.

To better analyze these similarities let us consider the low-pass filtered order parameter $R_f(t)$ defined in (15) for the SC. The comparison with $W(t)$ reported in Fig. 6 (b) clearly suggest that these two quantities are correlated in time. However, an almost perfect correlation is observable by considering the filtered synaptic current $I_f(t)$ as defined in (16). In this case $I_f(t)$ and $W(t)$ display an almost identical time evolution (see Fig. 6 (b)) thus revealing a strong correlation among the synaptic weights and the synaptic currents, at least by considering the corresponding (ensemble) averaged quantities.

In Fig. 6 (c) we reported also the corresponding LFP (see (16)). This exhibits minima with superimposed high frequency oscillations in the high activity phase, corresponding to the high synchronization, and maxima in the low synchronized phase. Despite this trace resembles strongly the spontaneous fluctuations observed in cortical activity of mammals during slow-wave sleep or during quiet wakefulness [1, 53], we should remark that our *up-states* and

down-states are characterized by a tonic firing of neurons with similar average ISIs.² In our case, the difference among these two states is mainly in the degree of synchronization of the population activity which is high (low) in the up-phase (down-phase). At variance with the experimentally observed activity in synchronized cortical states, typical of slow-wave sleep and quite wakefulness, which is characterized by up-phases (down-phases) associated to high level (absence) of firing activity [1].

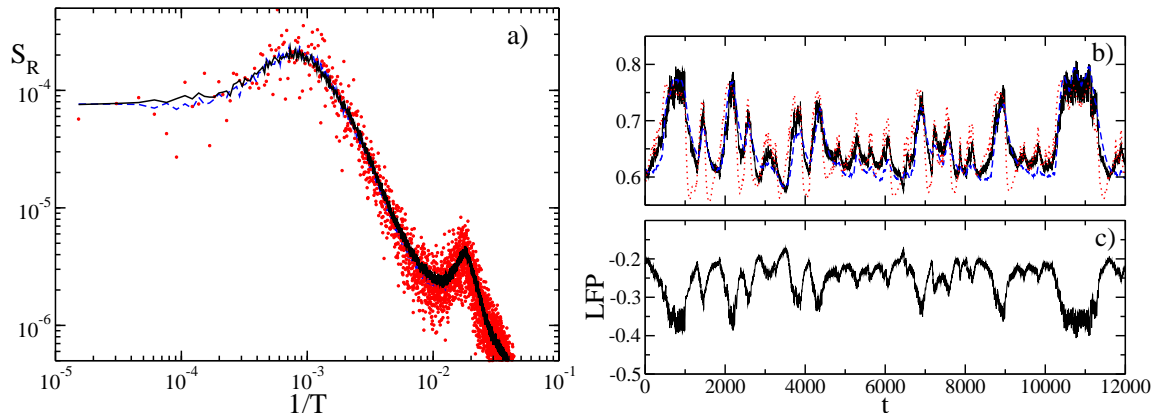


FIG. 6: (color online) (a) Power spectrum of the order parameter S_R versus the inverse of the period, for $a = 1.30$. The (black) solid line refers to $N = 100$, the (blue) dashed line to $N = 200$ and the (red) dots to $N = 400$. The power spectra have been obtained by the time trace of the parameter R sampled at regular intervals $\delta T = 1$ and for a time window $T_{tot} = 65,536$, the spectra are averaged over 200-400 different time windows at $N = 100$ and 200 over 10 windows for $N = 400$. (b) Time evolution of the filtered order parameter $R_f(t)$ (red dotted line), of the average synaptic current $I_f(t)$ (black solid line) and of the average synaptic weight $W(t)$ (blue dashed line) for $N = 500$. $R_f(t)$ and $I_f(t)$ have been arbitrarily shifted and rescaled to enhance the similarities with $W(t)$. (c) LFP as defined in (16) as a function of time. The reported results refer to $g = 0.4$, $\alpha = 9$, $d = p = 0.01$, $\tau_- = 3\tau_+ = 0.3$ and $w_{max} = 2$ and all the data are obtained after discarding a transient $\geq 10^5$.

IV. EFFECTIVE FREE ENERGY LANDSCAPE

A further characterization of this regime can be achieved by considering the probability density distribution $P(R)$ of the order parameter obtained by measuring R at regular time intervals δT during a long simulation, after discarding an initial transient time. In particular, we prefer to visualize the obtained results in term of the corresponding effective *free energy* landscape, as defined by $F(R) = -\log P(R)$ ³, as plotted in Fig. 7 (a). $F(R)$ reveals two minima at $R_L \simeq 0.3$ and $R_H \simeq 0.9$ corresponding to the LS and the HS regime, respectively. These two states are separated by a maximum located at $R_S \simeq 0.6$. The HS minimum is more pronounced and separated by a higher barrier ΔF from the saddle at R_S , this indicates that the system spends more time in the HS regime and that this state is characterized by a quite well defined level of synchronization. On the other hand the LS state corresponds to a broader minimum, reflecting the fact that the system in the LS regime visits states with levels of synchronization distributed over a broader range than in the HS state. From Fig. 7 (a) it is also evident that the large oscillations between LS and HS measured by $R(t)$ do not vanish in the thermodynamic limit, since $F(R)$ tends to an asymptotic profile already for $N > 100$.

The level of stability of the HS (LS) state can be measured in terms of the free energy barrier ΔF_H (ΔF_L) separating R_H (R_L) from the saddle R_S . These data are reported in Fig. 7 (b) for $d = p = 0.01$ and $\alpha = 9$ (and for $p = 2d = 0.02$ and $\alpha = 11$ in the inset) for a wide range of intrinsic excitability. We observe for the symmetric (asymmetric) case that finite barriers for both states exist only for $a \in [1.19; 1.46]$ ($a \in [1.22; 1.45]$), therefore in this interval HS and LS regime coexist. For $a \rightarrow 1.18$ ($a \rightarrow 1.21$) the HS barrier appears to diverge thus indicating that for smaller a -values the system is fully synchronized, while for $a \geq 1.48$ ($a \geq 1.47$) the two minima merge (the associated barriers vanish) in an unique LS state. These results are consistent with the analysis reported in Fig. 3 (a).

To determine if the observed oscillations between HS and LS persist by varying the relevant time scales (i.e. the synaptic time scale α^{-1} and the learning time windows), we have analyzed a large interval in the (α, τ_+) -plane. In

² We observe a variation of less than 10% of the ISI in the two states.

³ Here and in the following we assume an unitary scale for the energy.

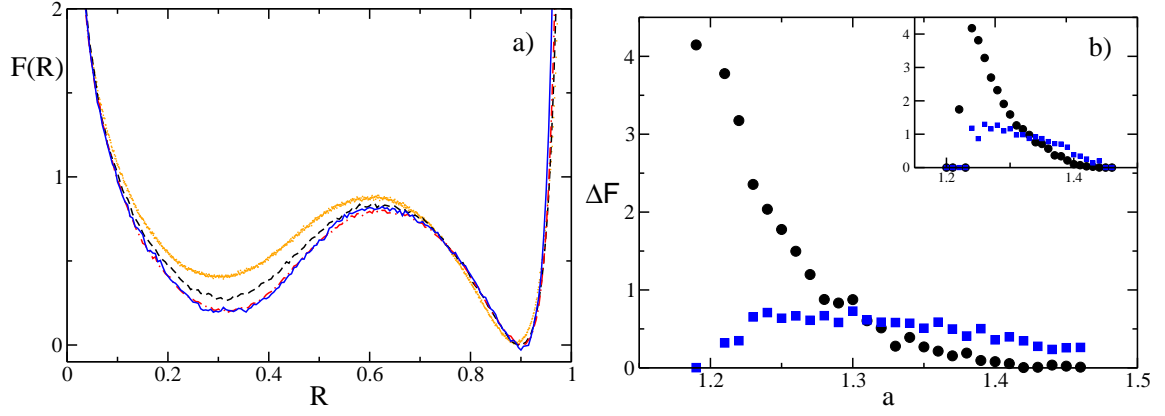


FIG. 7: (color online) (a) Free energy landscape $F(R) = -\log P(R)$ as obtained from the PDF of the order parameter $P(R)$ for $N = 50$ (orange) dots, $N = 100$ (black) dashed line, $N = 200$ (red) dot-dashed line and $N = 500$ (blue) solid line. The data are obtained by considering trajectories of duration $\simeq 2.7 \times 10^6 - 5.3 \times 10^6$ sampled at regular interval $\delta T = 1$, after discarding a transient $\simeq 10^7$ spikes. (b) Free energy barriers ΔF as a function of the intrinsic excitability a : the \bullet (\blacksquare) denote the barrier ΔF separating the minimum R_H (R_L) from the maximum R_S for a network of $N = 500$ neurons. The reported results refer to $g = 0.4$, $\tau_- = 3\tau_+ = 0.3$, $w_{max} = 2$, $\alpha = 9$ and $d = p = 0.01$, apart in the inset of panel (b) where we considered $p = 2d = 0.02$ and $\alpha = 11$.

particular, as suggested by the experimental evidences we fixed $\tau_- = 3\tau_+$ and we examined both the cases $d = p = 0.01$ and $p = 2d = 0.02$, with the other parameters held constant to $g = 0.4$ and $a = 1.3$. For each parameter set we have estimated the minimal free energy barrier ΔF_{min} between ΔF_H and ΔF_L , whenever ΔF_{min} is non zero this means that the neuronal dynamics oscillates between high synchronous and a low synchronous states, and therefore LFF oscillations are present. As shown in Fig. 8, the barriers are finite only in a limited stripe of the (α, τ_+) -plane, for smaller (larger) α -values the system is in the LS (HS) regime. In particular, for $0.02 \leq \tau_+ \leq 0.15$ one has $\Delta F_{min} > 0$ within the interval $\alpha \in [8; 10]$ ($\alpha \in [10; 12]$) for $d = p = 0.01$ ($p = 2d = 0.02$). Thus suggesting that the observation of LFFs is limited to synaptic rise/decay time $1/\alpha \simeq 0.1$ and it depends only slightly on τ_+ , at least in the examined range: by increasing τ_+ by a factor 5 the corresponding synaptic time needed to observe a finite ΔF_{min} grows only by 20%.

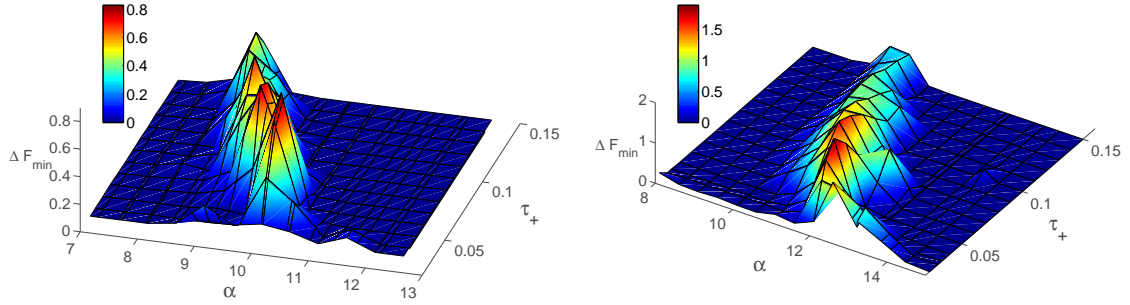


FIG. 8: (color online) Minimal free energy barriers ΔF_{min} as a function of α and τ_+ for $p = d = 0.01$ (a) and $p = 2d = 0.02$. The barrier heights are color coded, the scale is reported next to the corresponding figure. The reported results refer to $g = 0.4$, $a = 1.3$, $N = 200$, $\tau_- = 3\tau_+$, and $w_{max} = 2$.

V. CONSTRAINED SIMULATIONS

As previously noticed it seems that, at least at a mean field level, the dynamics of the synaptic weights and the synchronization of the firing events are somehow related. In order to clarify this relationship, if any, we will examine the neuronal population dynamics *decoupled* from the evolution of the average synaptic strength by performing CSs.

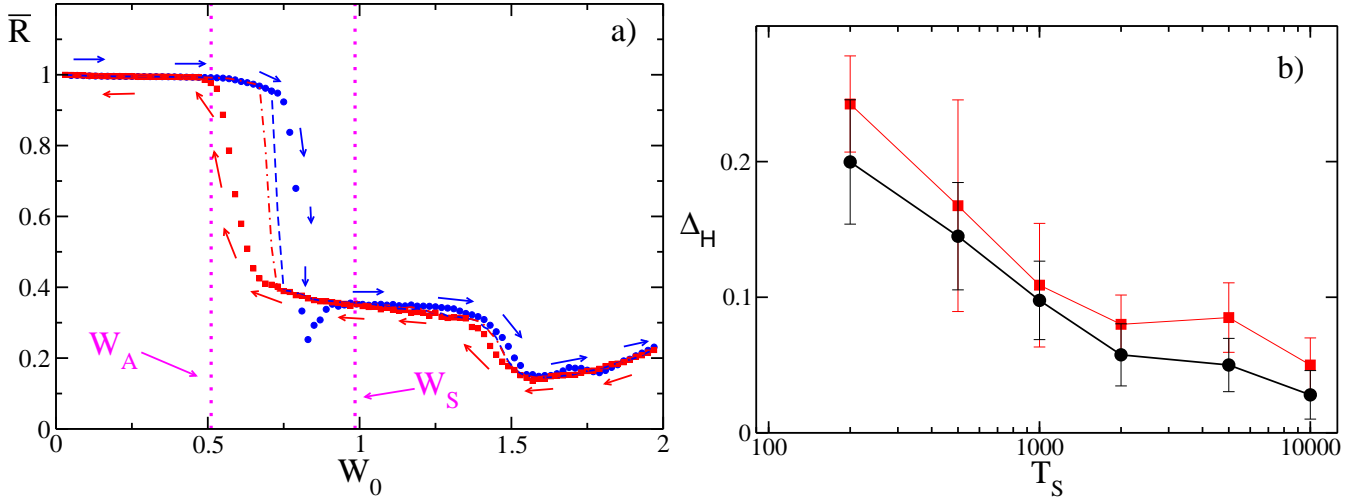


FIG. 9: (Color online) (a) Plots of \bar{R} vs W_0 as obtained during constrained simulations of duration T_S for increasing (● and --) and decreasing (■ and ·-) W_0 . The symbols correspond to $T_S = 200$ and the lines to $T_S = 10,000$. The magenta dotted vertical lines indicate the fixed point values W_A and W_S . Results averaged over 100 different initial conditions and $\delta W_0 = 0.02$. The data refer to $p = 0.01$ and $\alpha = 9$. (b) Width of the hysteretic loop Δ_H as a function of T_S for $p = 0.01$, $\alpha = 9$ (black circle) and $p = 0.02$, $\alpha = 11$ (red squares), the error bars have been estimated by measuring Δ_H for 250 (33) different initial conditions, respectively. All the data are for $d = 0.01$, $\tau_- = 3\tau_+ = 0.3$, $g = 0.4$, $a = 1.3$, $N = 200$.

During this kind of simulation the average synaptic weight is maintained constant and equal to a fixed value W_0 . In particular, we set initially $W_0 = 0$ and follow the evolution of the system for a time span T_S . Then, we perform a new simulation of duration T_S , starting from the last configuration of the previous run, with an increased synaptic weight $W_0 = \Delta W_0$. We repeat this procedure by increasing W_0 at regular steps ΔW_0 until W_0 reaches the maximal allowed value, namely w_M . By applying the reverse protocol, W_0 is successively decreased (always at steps of ΔW_0) until it returns to zero. During each single simulation we measure the average order parameter \bar{R} only over the second half of the run (therefore on a time interval $T_S/2$), this in order to allow the system to relax after each modification of W_0 . The corresponding results are shown in Fig. 9 (a) for $T_S = 200$ and $T_S = 10,000$. In this manner, W is held fixed, while the individual w_{ij} are essentially free to evolve.

At low W_0 the system is fully synchronized $\bar{R} \simeq 1$, by increasing the average synaptic weight the order parameter drops to a LS state above a critical value $W_0^{(1)}$. Furthermore, the system resynchronizes, by decreasing W_0 , at a lower synaptic weight value, namely $W_0^{(2)} < W_0^{(1)}$. This seems to indicate that the transition is discontinuous and hysteretic, however by increasing from $T_S = 200$ to $T_S = 10,000$ the transition remains discontinuous, but the width of the hysteretic loop $\Delta_H = W_0^{(2)} - W_0^{(1)}$ shrinks noticeably, as evident from Fig. 9 (a). To better investigate this point, we report Δ_H as a function of T_S in Fig. 9 (b), these data seem to suggest that Δ_H will vanish for adiabatic transformations of W_0 , corresponding to $T_S \rightarrow \infty$.

However, since we are interested in characterizing the transition between HS and LS observed during LFFs and since each oscillation in $R(t)$ ($W(t)$) takes place on a finite time the limit $T_S \rightarrow \infty$ is not of interest for this analysis. However, it is not trivial to estimate which is a meaningful T_S -value to employ in the CSs to compare the obtained results with those of the corresponding USs. A first constraint on T_S is that it should be sufficiently long with respect to the period of the HFF, this in order to get rid of the fast oscillations of $R(t)$ during CSs. On the other hand, the variation of W_0 , performed during CSs, should be done on time scales of the order of the period of the LFFs. To be more specific, let us focus on the SC. For these parameter values, HFFs occur on time scales $T_{HFF} \simeq 50 - 60$, therefore the first request is that $T_S \gg T_{HFF}$. Furthermore, the period of the LFFs is $T_{LFF} \simeq 1,000 - 2,000$. For the AC, the time scales associated to LFFs and HFFs are faster. As a matter of fact, to be on the safe side we have employed $T_S \simeq 200 - 1,000$.

VI. MEAN-FIELD PREDICTION OF SYNAPTIC WEIGHT DYNAMICS

We now address the influence of the level of synchrony of the neuronal population, as measured by the order parameter R , on the synaptic weight dynamics, using a mean-field analysis for W . In particular, we examine the dynamics of W in the two extreme cases of fully synchronized and asynchronous evolution of the network.

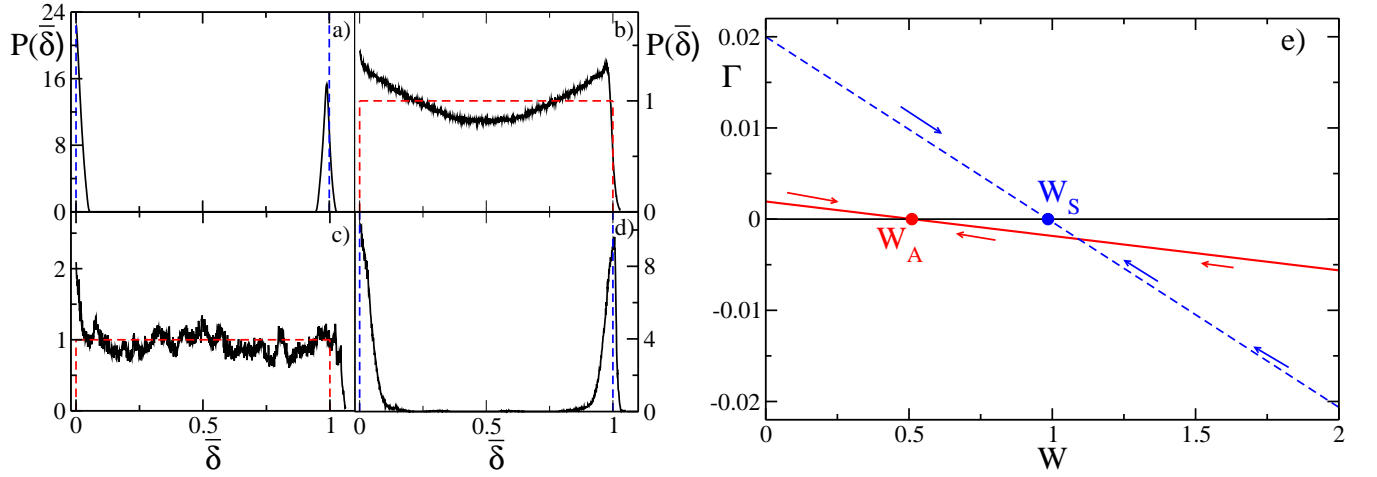


FIG. 10: (color online) Probability distribution functions $P(\bar{\delta})$ as a function of the renormalized time differences $\bar{\delta}_{ij} = \delta_{ij} / \langle ISI \rangle$, where $\langle ISI \rangle$ is the average inter-spike interval measured for the considered state. The reported PDF refer to $a = 1.09$ (a); $a = 1.7$ (b) and $a = 1.3$ (c) and (d). For the latter case, the distributions have been obtained during an unconstrained simulation by considering the $N \times (N - 1)$ δ_{ij} values associated to the last N spikes preceding a strongly (weakly) synchronized state corresponding to an order parameter value $R \simeq 0.11$ (c) ($R \simeq 0.98$ (d)). The -- refer to P_S in (a) and (d), while the - - refer to P_A in (b) and (d). (e) Γ versus W for the asynchronous and the synchronized case: namely Γ_A (-) and Γ_S (--). The arrows denote the direction of the evolution of $W(t^+)$ due to the modifications induced by $\Gamma(W(t^-))$. The \bullet (\bullet) indicates $W_A \simeq 0.51$ ($W_S \simeq 0.985$). The other parameters of the simulations are $\alpha = 9$, $\tau_- = 3\tau_+ = 0.30$, $d = p = 0.01$, $g = 0.4$ and the network size is $N = 500$

From Eqs. (6,7) and by following the approach described in [38], one can obtain the average synaptic weight modification Γ , associated to each presynaptic spike,

$$\Gamma(t) = p(w_M - W) \int_0^\infty d\delta P(\delta) e^{\frac{-\delta}{\tau_+}} - dW \int_{-\infty}^0 d\delta P(-\delta) e^{\frac{\delta}{\tau_-}} \quad (18)$$

where $P(\delta)$ is the PDF of the time differences δ between postsynaptic and presynaptic firing times. To test the predictive value of Eq. (18), we have measured from USs $P(\delta)$ at regular time intervals Δt , thanks to these data we can estimate the evolution of the synaptic weight at regular time intervals, as $W(t + \Delta t) = W(t) + \Gamma(t)$. This reconstruction gives a quite good estimation of the true evolution for SC (see the dotted blue line in Fig. 5 (a)). However the agreement declines for the AC, in this case the mean-field evolution still catches the oscillations of $W(t)$ with the correct periods, but it overestimates the minimal values reached by the synaptic weights, as shown in Fig. 5 (b). We have verified that the mean field prediction remains good in the symmetric case $p = d$, even by doubling the value of p , and also by considering a situation with depression prevailing on potentiation, namely $d = 2p$. The origin of the partial failure of the mean-field prediction (18) could be related to the fact the collective dynamics becomes faster in the AC, as discussed in Sect. III. Despite this, the overall picture seems still to work also when potentiation is larger than depression, and the mechanism at work for the generation of LFF seems the same in the SC and AC, as detailed in Sect. VII.

By assuming that the postsynaptic neuron is firing with period T_0 , we are able to derive the time difference distribution $P(\delta)$ for the two limiting cases: fully synchronized and asynchronous dynamics. In the fully synchronized (asynchronous) situations we expect a distribution of the form $P_S(\delta) = \mathcal{D}(\delta) + \mathcal{D}(\delta - T_0)$ ($P_A(\delta) = 1/T_0$) defined in the interval $[0, T_0]$. Here \mathcal{D} denotes a Dirac delta function. These guesses are essentially confirmed by direct USs as shown in Fig. 10. In particular, the data reported in Fig. 10 (a) (Fig. 10 (b)) refer to a high (low) synchronized state corresponding to $a = 1.09$ ($a = 1.7$). On the other hand the results shown in Fig. 10 (c) and (d) refer to the same state, corresponding $a = 1.3$, where $P(\delta)$ is measured by considering the δ_{ij} values associated to the last N spikes preceding a strongly (weakly) synchronized phase with associated an order parameter value $R \simeq 0.11$ (c) ($R \simeq 0.98$ (d)). Therefore, at least in these two cases, we can derive an analytic estimation of Γ . By assuming that the post-synaptic neuron fires with constant period T_0 we can perform the integrals appearing in (18) obtaining the following results.

A. Asynchronous dynamics

In this situation $P(\delta) = P_A(\delta)$ and we can rewrite (18) as follows

$$\Gamma_A = \frac{1}{T_0} \left[p\tau_+(2 - W) \left(1 - e^{-T_0/\tau_+} \right) - dW\tau_- \left(1 - e^{-T_0/\tau_-} \right) \right] . \quad (19)$$

As shown in Fig. 10 (e), Γ_A vanishes for $W = W_A$ and it is positive (negative) for $W < W_A$ ($W > W_A$), therefore for the dynamics of $W(t)$

$$W_A = \frac{2P}{S + P} , \quad P = \tau_+ \left(1 - e^{-T_0/\tau_+} \right) , \quad D = \tau_- \left(1 - e^{-T_0/\tau_-} \right) \quad (20)$$

is a stable fixed point. The value of W_A only depends on the STDP parameters and T_0 , by assuming that the period T_0 is equal to the average inter-spike interval, we can estimate the value of this fixed point. As shown in Fig. 12 this prediction gives a good estimation of the W values in the low synchronized regime (corresponding to $a > 1.6$) both for $p = d$ as well as for $p = 2d$.

B. Fully synchronized dynamics

For the fully synchronized situation $P(\delta) = P_S(\delta)$ and (18) becomes

$$\Gamma_S = p(2 - W) \left(1 + e^{-T_0/\tau_+} \right) - dW \left(1 + e^{-T_0/\tau_-} \right) . \quad (21)$$

As reported in Fig. 10 (e), Γ_S vanishes for $W = W_S$ and it is positive (negative) for $W < W_S$ ($W > W_S$), therefore the solution

$$W_S = \frac{2\tilde{P}}{\tilde{P} + \tilde{S}} , \quad \tilde{P} = 1 + e^{-T_0/\tau_+} , \quad \tilde{D} = 1 + e^{-T_0/\tau_-} , \quad (22)$$

represents an stable fixed point. Also in this situation by setting $T_0 = \langle ISI \rangle$ we can obtain a numerical estimation of W_S , as clearly shown in Fig. 12. This represents an upper bound for W for any studied regime, while $W \rightarrow W_S$ only for $a \rightarrow 1$, corresponding to the state of maximal synchronization.

To summarize, in both cases Γ vanishes for a finite value of the average synaptic weight, namely W_S (W_A) for the synchronized (asynchronous) situation. Additionally, for $W < W_S$ ($W > W_A$) the synapses are on average potentiated (depressed), while a similar mechanism rules for the asynchronous case. This implies that W_S (W_A) is a stable attractive point for the dynamics of W in the synchronized (asynchronous) regime. All these results apply in the symmetric (asymmetric) case $p = d = 0.01$ ($p = 2d = 0.02$), whenever $\tau_- = 3\tau_+ = 0.30$. However, in general the system will not be completely synchronized or asynchronous and the distribution $P(\delta)$ will lie in between the extreme cases represented by P_S and P_A , therefore we expect that the values of W will be bounded within the interval $[W_A, W_S]$. This expectation is fully confirmed for $p = d = 0.01$, as shown in Fig. 12 (a), while for $p = 2d = 0.02$ $W < W_S$ for any value of the intrinsic excitability a , but in the intermediate regime (namely, $1.25 < a < 1.50$) W can attain values somehow lower than W_A . This result is due to the not perfectly good predictive power of the mean field approach in this specific case, as already stated previously.

VII. SISYPHUS EFFECT

We have now all the ingredients needed to explain the LFFs reported previously and to single out the mechanism responsible for such behavior. Let us suppose that initially the system is in the HS phase with an associated average low coupling value $W < W_0^{(1)}$. In this regime the attractive fixed point W_S is larger than the transition point $W_0^{(1)}$ (see Fig. 9 (a)). Therefore W increases and tends towards W_S , until $W > W_0^{(1)}$, at which point the system starts to desynchronize and to approach the LS state, the value of R dropping. In this desynchronizing stage the distribution $P(\delta)$ becomes almost flat (see Fig. 10 (c)) and the attractive point for the synaptic evolution will now be W_A , which is located below $W_0^{(2)}$ (as shown in Fig. 9 (a)). The synaptic plasticity decreases W in order to reach W_A , but when the average synaptic weight crosses $W_0^{(2)}$ the neurons begins to resynchronize. This brings the system

back to the HS state from where it started and the cycle can now be repeated. The cycle will continue indefinitely, and is the essence of the Sisyphus Effect.

One should remark that the above arguments are approximate, because the system is never exactly fully synchronized or desynchronized. Instead the network passes through a continuum of states, each associated with a different fixed point in W -space. The crucial ingredient for the emergence of the SE is that the fixed points corresponding to the HS (LS) phase are larger than the transition point $W_0^{(1)}$ (smaller than $W_0^{(2)}$). As we have verified that this is indeed the case, the described mechanism can be considered as still effective.

To perform a further test of the validity of our analysis, we measure the probability distribution function (PDF) of the order parameter R conditioned to the fact that W was increasing (decreasing) during an US. From the PDFs we can derive the corresponding free energy profiles $F_I(R)$ and $F_D(R)$, which are reported in Fig. 11. From the figure F_I has a principal minimum at R_H , while F_D has an absolute minimum at R_L . Both profiles reveal a shoulder at intermediate R values. These results confirm that the equilibrium attractive values for W are located opposite to the transition points, because when the system is in the HS (LS) regime the synaptic weights increase (decrease) continuously trying to reach the corresponding fixed points.

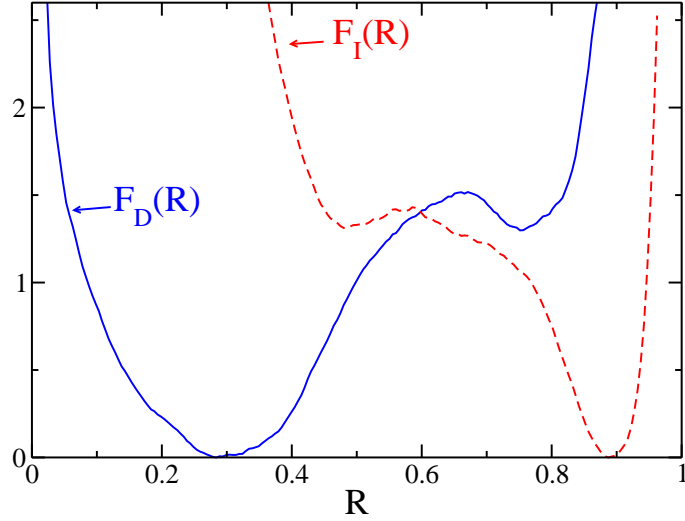


FIG. 11: (color online) Conditional free energy profiles for R : $-$ refers to $F_D(R)$, while $- -$ to $F_I(R)$. The PDF has been obtained during USs by averaging over measurements of R obtained at regular time intervals $\Delta T = 1$. The data correspond to $N = 2000$, $\alpha = 9$, $g = 0.4$, $a = 1.3$, $p = d = 0.01$, $\tau_- = 3\tau_+ = 0.3$.

As a final analysis, we have verified the validity of the SE over a wide range of intrinsic excitabilities for the symmetric and asymmetric case. We expect that the SE appears whenever the transition values $W_0^{(1)}$ and $W_0^{(2)}$ lie within the interval $[W_A, W_S]$. Therefore, we have measured the transition values $W_0^{(1)}$ and $W_0^{(2)}$ and the corresponding fixed points for a large interval of intrinsic excitabilities, namely $1 < a \leq 2$ for $p = d = 0.01$ and $p = 2d = 0.02$ (see Fig. 12). For, $p = d$ ($p = 2d$) the transition is hysteretic in the interval $a \in]1, 1.40]$ ($a \in]1, 1.45]$) while for larger a -values $W_0^{(1)}$ and $W_0^{(2)}$ are essentially coincident. Furthermore, for $a \leq 1.18$ ($a \leq 1.17$) $W_0^{(1)} \geq W_S$, while for $a \geq 1.50$ ($a \geq 1.51$) $W_A \geq W_0^{(1)}, W_0^{(2)}$. Furthermore, the W distributions measured during USs are reported in Fig 12 as shaded areas and they include the transition interval $[W_0^{(1)}, W_0^{(2)}]$ for $1.20 \leq a \leq 1.48$ ($1.20 \leq a \leq 1.51$). In the AC one observes that, in the range of parameters where the Sisyphus mechanism is at work, the measured W can be smaller than W_A , instead outside this region W_A always represents a lower bound for the distribution of the W . This is in line with what previously reported in Sec. VI concerning the predictive value of Eq.(18) and it points out that one should go beyond the mean-field approximation to get a better reproduction of the W dynamics, at least in the AC.

As previously shown in Fig. 7 (b) the free energy $F(R)$ reveals the coexistence of two minima, corresponding to the competing HS and LS states, within the interval $a \in [1.19 : 1.46]$ ($a \in [1.22 : 1.45]$) for the symmetric (asymmetric) case. These results clearly indicate that the Sisyphus Effect is responsible for the LFFs observed in the dynamics of our network.

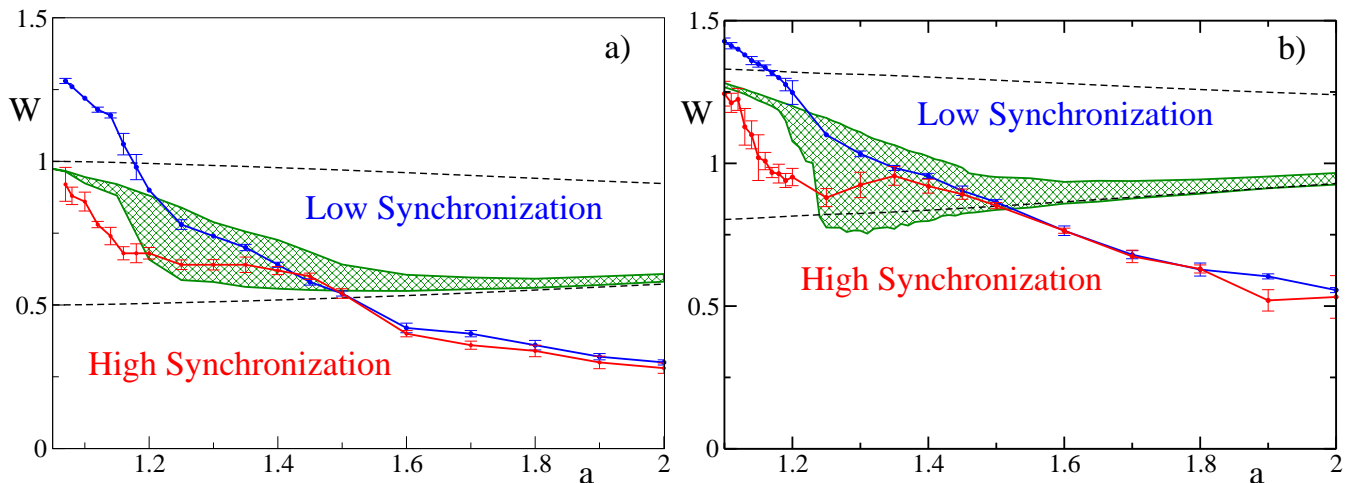


FIG. 12: (color online) Average synaptic plasticity W versus intrinsic excitability a . The shaded area indicates the distribution of the W values measured during USs. The upper blue (low red) line represents $W_0^{(1)}$ ($W_0^{(2)}$). The error bars have been evaluated over 5 different realizations of the CSs. The upper (lower) dashed black line represents the fixed point values W_S (W_A). The data refer to (a) $p = d$ and $\alpha = 9$; (b) $p = 2d$ and $\alpha = 11$; while the other parameters are set to $N = 200$, $g = 0.4$, $T = 1000$, $d = 0.01$, $\tau_- = 3\tau_+ = 0.3$.

VIII. CONCLUSIONS

In this paper we have reported a simple deterministic mechanism, the Sisyphus Effect, responsible for the onset of irregular collective oscillations between asynchronous and synchronous states in excitatory neural networks with STDP. The transition between the two states are driven by STDP: the synaptic weights tend to relax towards their equilibrium values, which in turn are determined by the synchrony in the neural population.

For intermediate values of the synaptic characteristic time, the system is fully synchronized for sufficiently small synaptic weights, while it becomes asynchronous above a critical coupling. However, for synchronized (desynchronized) neural activities the synaptic weights tend towards large (small) equilibrium values corresponding to asynchronous (synchronous) evolution. The activity of the network can be schematized as that of a one dimensional order parameter evolving on a free energy landscape displaying two coexisting equilibria. Depending on the small (large) values of the synaptic weights the landscape is tilted towards the strongly (weakly) synchronized state, thus becoming the attractive equilibrium for the dynamics. On the other hand, the synchronized (desynchronized) neural activity increases (reduces) the weights until their values force the landscape to tilt in the opposite direction. This drives both the observables into a never ending cyclic behavior.

The SE should be observable in pulse coupled neural networks for usual STDP whenever excitation has a desynchronizing effect. On one hand, this is, in general, verified for any kind of neuronal response (type I or type II) for sufficiently slow synaptic interactions [34, 35]. On the other hand, for fast excitatory synapses, we expect that for temporally inverted STDP rules [54] the Sisyphus effect should be active. Furthermore, we have shown that this effect is present also for biologically relevant choices of the STDP parameters and the collective oscillations occurs on timescales corresponding to infraslow oscillations observed in the brain dynamics. In relation to this, it is very interesting to note that the authors of refs. [6, 7] described infraslow fluctuations in the excitability of real neural networks. Such fluctuations could be explained by the slow oscillations of the synaptic couplings as caused by the Sisyphus Effect.

Ultralow rhythms have been previously reproduced in an excitatory network composed of fully coupled conductance based neurons [55]. In particular, the authors proposed a mechanism, based on retrograde endocannabinoid signaling, which was quite similar to the Sisyphus Effect. Also in Ref. [55] high level of synchrony induced a feedback mechanism based on the evolution of a mean-field variable which leads to a decoupling of the neurons. Furthermore, whenever the neurons desynchronize the suppression mechanism was removed and the populations can evolve towards its synchronous activity. However, at variance with the SE the evolution time scale of the mean field control parameter was phenomenologically set to be $\simeq 10 - 100$ s.

The reported deterministic collective dynamics is absolutely not trivial, and deserves further analysis to understand if the observed collective motion, which is clearly chaotic from a microscopic point of view, can be considered a further example of collective chaos, similar to the one recently reported for two coupled sub-populations of neurons [56].

Acknowledgments

We acknowledge illuminating discussions with B. Lindner, L. Shimansky-Geier, M. Wolfrum, A. Politi, Y. Maistrenko, S. Lepri, S. Luccioli, M. Bazhenov, J. Berke, S. Coombes, D. Angulo-Garcia. AT thanks the VELUX Visiting Professor Programme 2011/12 and the Aarhus Universitets Forskningsfond for the support received during his stays at the University of Aarhus (Denmark). This work is part of the activity of the Marie Curie Initial Training Network 'NETT' project # 289146 financed by the European Commission and it has been partially supported by the DFG - Deutsche Forschungsgemeinschaft in the framework of the Collaborative Research Center SFB 910.

-
- [1] K. D. Harris and A. Thiele, *Nat Rev Neurosci* **12**, 509 (2011).
 - [2] E. Van Someren, *Slow Brain Oscillations of Sleep, Resting State and Vigilance*, vol. 193 (Elsevier, 2011).
 - [3] M. M. Steriade and R. W. McCarley, *Brain control of wakefulness and sleep* (Springer, 2007).
 - [4] M. Okun, A. Naim, and I. Lampl, *The Journal of Neuroscience* **30**, 4440 (2010).
 - [5] G. Buzsáki, *Neuroscience* **31**, 551 (1989).
 - [6] S. Monto, S. Palva, J. Voipio, and J. M. Palva, *The Journal of neuroscience* **28**, 8268 (2008).
 - [7] S. Vanhatalo, J. M. Palva, M. Holmes, J. Miller, J. Voipio, and K. Kaila, *Proceedings of the National Academy of Sciences of the United States of America* **101**, 5053 (2004).
 - [8] R. N. Romcy-Pereira, J. P. Leite, and N. Garcia-Cairasco, *Epilepsy & Behavior* **14**, 47 (2009).
 - [9] P. Tass and M. Majtanik, *Biological Cybernetics* **94**, 58 (2006).
 - [10] Y. L. Maistrenko, B. Lysyansky, C. Hauptmann, O. Burylko, and P. A. Tass, *Physical Review E* **75**, 066207 (2007).
 - [11] E. V. Lubenov and A. G. Siapas, *Neuron* **58**, 118 (2008).
 - [12] M. Ciszak and M. Bellesi, *Chaos: An Interdisciplinary Journal of Nonlinear Science* **21**, 043119 (2011).
 - [13] G. Mongillo, D. Hansel, and C. van Vreeswijk, *Phys. Rev. Lett.* **108**, 158101 (2012).
 - [14] H. Markram, J. Lübke, M. Frotscher, and B. Sakmann, *Science* **275**, 213 (1997).
 - [15] G. Q. Bi and M. M. Poo, *The Journal of Neuroscience* **18**, 10464 (1998).
 - [16] D. Debanne, B. H. Gähwiler, and S. M. Thompson, *The Journal of Physiology* **507**, 237 (1998).
 - [17] S. Song, K. D. Miller, and L. F. Abbott, *Nature Neuroscience* **3**, 919 (2000).
 - [18] R. C. Froemke and Y. Dan, *Nature* **416**, 433 (2002).
 - [19] H.-X. Wang, R. C. Gerkin, D. W. Nauen, and G.-Q. Bi, *Nature Neuroscience* **8**, 187 (2005).
 - [20] J. Sjöström and W. Gerstner, *Scholarpedia* **5(2)**, 1362 (2010).
 - [21] G. Bi and M. Poo, *Annual review of neuroscience* **24**, 139 (2001).
 - [22] G. Q. Bi and H. X. Wang, *Physiology & behavior* **77**, 551 (2002).
 - [23] R. Froemke and Y. Dan, *Nature* **416**, 433 (2002).
 - [24] T. Nowotny, V. P. Zhigulin, A. I. Selverston, H. D. I. Abarbanel, and M. I. Rabinovich, *The Journal of Neuroscience* **23**, 9776 (2003).
 - [25] V. P. Zhigulin, M. I. Rabinovich, R. Huerta, and H. D. I. Abarbanel, *Physical Review E* **67**, 021901+ (2003).
 - [26] V. Zhigulin and M. Rabinovich, *Neurocomputing* **58-60**, 373 (2004).
 - [27] C. C. Chen and D. Jasnaw, *Physical Review E* **81**, 011907 (2010).
 - [28] C. C. Chen and D. Jasnaw, *Phys. Rev. E* **84**, 031908 (2011).
 - [29] O. V. Popovych, S. Yanchuk, and P. A. Tass, *Scientific reports* **3** (2013).
 - [30] J.-P. P. Pfister and P. A. Tass, *Frontiers in computational neuroscience* **4** (2010).
 - [31] K. Mikkelsen, A. Imperato, and A. Torcini, *Physical Review Letters* **110**, 208101 (2013).
 - [32] L. F. Abbott and C. van Vreeswijk, *Phys. Rev. E* **48**, 1483 (1993).
 - [33] W. Rall, R. E. Burke, T. G. Smith, P. G. Nelson, and K. Frank, *Journal of Neurophysiology* **30**, 1169 (1967).
 - [34] C. Vreeswijk, L. F. Abbott, and G. Bard Ermentrout, *Journal of Computational Neuroscience* **1**, 313 (1994).
 - [35] D. Hansel, G. Mato, and C. Meunier, *Neural Computation* **7**, 307 (1995).
 - [36] C. van Vreeswijk, *Physical Review E* **54**, 5522 (1996).
 - [37] G. G. Turrigiano, *Cell* **135**, 422 (2008).
 - [38] E. M. Izhikevich and N. S. Desai, *Neural Comput.* **15**, 1511 (2003).
 - [39] E. Bienenstock, L. Cooper, and P. Munro, *The Journal of Neuroscience* **2**, 32 (1982).
 - [40] S. Olmi, R. Livi, A. Politi, and A. Torcini, *Physical review. E, Statistical, nonlinear, and soft matter physics* **81** (2010).
 - [41] A. Winfree, *The Geometry of Biological Time* (Springer-Verlag, Berlin-Heidelberg-New York, 1980).
 - [42] Y. Kuramoto, *Chemical Oscillations, Waves, and Turbulence*, Dover Books on Chemistry Series (Dover Publications, New York, 2003).
 - [43] P. L. Nunez, *Electric fields of the brain: the neurophysics of EEG* (Oxford University Press, 2006).
 - [44] C. Hauptmann and P. Tass, *Journal of neural engineering* **6**, 016004 (2009).
 - [45] O. V. Popovych and P. A. Tass, *Progress in biophysics and molecular biology* **105**, 98 (2011).
 - [46] G. Buzsáki, C. A. Anastassiou, and C. Koch, *Nature Reviews Neuroscience* **13**, 407 (2012).
 - [47] R. Zillmer, R. Livi, A. Politi, and A. Torcini, *Phys. Rev. E* **76**, 046102 (2007).

- [48] M. Rosenblum and A. Pikovsky, Physical review letters **98**, 064101 (2007).
- [49] A. Pikovsky and M. Rosenblum, Physica D: Nonlinear Phenomena **238**, 27 (2009).
- [50] A. A. Temirbayev, Z. Z. Zhanabaev, S. B. Tarasov, V. I. Ponomarenko, and M. Rosenblum, Physical Review E **85**, 015204 (2012).
- [51] P. K. Mohanty and A. Politi, Journal of Physics A: Mathematical and General **39**, L415 (2006).
- [52] M. Tsodyks, I. Mitkov, and H. Sompolinsky, Phys. Rev. Lett. **71**, 1280 (1993).
- [53] S. Chauvette, S. Crochet, M. Volgushev, and I. Timofeev, The Journal of Neuroscience **31**, 14998 (2011).
- [54] J. J. Letzkus, B. M. Kampa, and G. J. Stuart, The Journal of neuroscience **26**, 10420 (2006).
- [55] J. Hlinka and S. Coombes, Physical review letters **104**, 068101 (2010).
- [56] S. Olmi, A. Politi, and A. Torcini, EPL (Europhysics Letters) pp. 60007+ (2010).
- [57] M. C. Van Rossum, G. Bi, and G. G. Turrigiano, The Journal of Neuroscience **20**, 8812 (2000).
- [58] G. G. Turrigiano, K. R. Leslie, N. S. Desai, L. C. Rutherford, and S. B. Nelson, Nature **391**, 892 (1998).
- [59] R. J. O'Brien, S. Kamboj, M. D. Ehlers, K. R. Rosen, G. D. Fischbach, and R. L. Haganir, Neuron **21**, 1067 (1998).
- [60] M. Derchansky, S. Jahromi, M. Mamani, D. Shin, A. Sik, and P. Carlen, The Journal of physiology **586**, 477 (2008).
- [61] D. Sterratt, B. Graham, A. Gillies, and D. Willshaw, *Principles of Computational Modelling in Neuroscience* (Cambridge University Press, 2011), 1st ed.
- [62] P. Dayan and L. F. Abbott, *Theoretical Neuroscience: Computational and Mathematical Modeling of Neural Systems* (The MIT Press, 2001), 1st ed.

Appendix A: Synaptic weights distributions

In this appendix we investigate the shape and the stationarity of the probability density distributions of the synaptic weights $P(w_{ij})$ for various regimes. The distributions are stationary in the regimes of High and Low Synchronization, namely when the Sisyphus Effect is absent. In these cases, they do not depend on the initial conditions and converge to the distribution reported in Fig. 13 (a) and (b), corresponding to High and Low Synchronization, respectively. However, these distributions have some different features: in the HS regime $P(w_{ij})$ is essentially symmetric and peaked around $w_{ij} = 1$; in the LS regime $P(w_{ij})$ is a skewed distribution peaked at $w_{ij} \simeq 0.5$ and with a tail extending towards larger values. These results are consistent with the findings reported in [57], where the authors have shown that uncorrelated inputs lead to a unimodal distribution with a positive skew (similar to the one reported in Fig. 13 (b)), consistently with experimental findings [58, 59]. Furthermore, in [57] it has been also shown that correlation among the inputs lead to a potentiation of the synapses and to a more symmetric distribution. This is also the case for our model: the distribution becomes more symmetric and peaked at a larger w_{ij} -value when passing from the LS regime to the HS, characterized by a larger degree of correlation among the neurons (see Fig. 13 (a,b)).

The situation changes completely in presence of the Sisyphus Effect, since in this case the level of synchronization (of correlation) changes continuously in time leading to a non-stationary distribution $P(w_{ij})$. In particular, in Fig. 13 (c,d) we reported the distributions estimated when the system is almost completely desynchronized (synchronized) corresponding to $R \simeq 0.1$ ($R \simeq 0.9$) shown in Fig. 13 (c) (Fig. 13 (d)). These distributions have been obtained by averaging over 20 different configurations of the system characterized by the desired level of synchronization. It is evident that also in this case the synchronization favours the potentiation of the synapses leading to the emergence of a positive tail extending towards w_M (see Fig. 13 (d)). However, in both situations two peaks are present in the distributions at $w_{ij} \simeq 1$ and $w_{ij} < 0.5$, indicating the coexistence of two subpopulations in the system resembling the ones found in the HS and LS regime shown in Fig. 13 (a,b). This result suggests that the Sisyphus Effect occurs on time scales which are short with respect to the ones required by the synapses to relax towards an unimodal distribution. The distribution of the weights evolve in time recursively switching from the distribution reported in panel (d) of Fig. 13 to the one in panel (c) and so on, for ever. It is important to stress that $P(w_{ij})$ does not tend to split in two groups peaked at $w_{ij} = 0$ and $w_{ij} = w_M$, as it would occur in the models of STDP where potentiation and depression modify the synaptic weights by a fixed amount, irrespective of the actual value of w_{ij} [57].

Appendix B: Physical Units

The model introduced in the paper contained only adimensional units, since these are more convenient to perform numerical simulations. However, the evolution equation for the membrane potential (1) can be easily re-expressed in terms of dimensional variables as follows

$$\tau_m \dot{\mathcal{V}}_j(\tilde{t}) = \mathcal{R}_{in} \mathcal{J}^b - \mathcal{V}_j(\tilde{t}) + \tau_m \mathcal{G} \mathcal{E}_j(\tilde{t}) \quad j = 1, \dots, N \quad ; \quad (\text{B1})$$

where $\tau_m = 40$ ms is the membrane time constant (as reported in [60] for pyramidal cells in brain area CA1 of hippocampus), \mathcal{R}_{in} is the membrane resistance, \mathcal{J}^b represents the neural excitability, due to contributions from

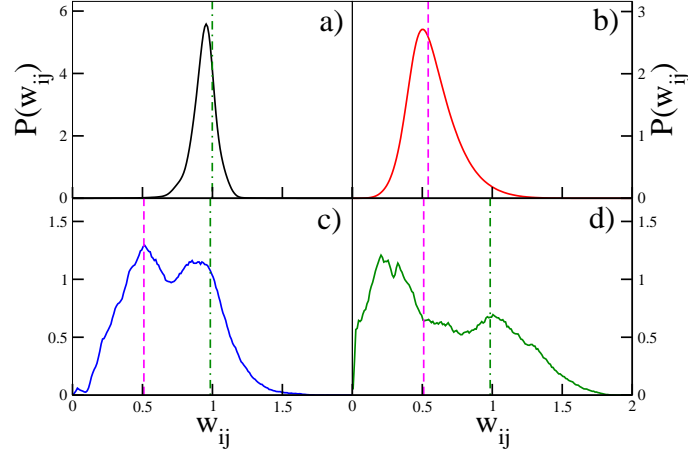


FIG. 13: (color online) Probability density distributions $P(w_{ij})$ for $a = 1.09$ (a), $a = 1.7$ (b) and for $a = 1.3$ measured for small (large) synchronization values $R \simeq 0.1$ ($R \simeq 0.9$) corresponding to panels (c) and (d), respectively. These latter distributions have been obtained by averaging over 20 different configurations of similar R -value (the 20 highest and lowest during a long run, respectively), while the other two are single snapshot. The vertical magenta dashed (green dot-dashed) lines indicate the mean-field equilibrium points W_A (W_S) in the considered cases. The parameters are $N = 500$, $\alpha = 9$, $g = 0.4$, $a = 1.3$, $p = d = 0.01$, $\tau_- = 3\tau_+ = 0.3$.

neurons lying outside the local network and projecting on them. Furthermore, $\tilde{t} = t \cdot \tau_m$, the inverse pulse-width is $\tilde{\alpha} = \alpha/\tau_m$, the field $\mathcal{E}_j = E_j/\tau_m$ has the dimensionality of a frequency and \mathcal{G} of a potential.

For the other parameters/variables the transformation to physical units is simply given by

$$\mathcal{V}_j = \mathcal{V}_r + (\mathcal{V}_{th} - \mathcal{V}_r)V_j \quad (\text{B2})$$

$$\mathcal{R}_{in}J^b = \mathcal{V}_r + (\mathcal{V}_{th} - \mathcal{V}_r)a \quad (\text{B3})$$

$$\mathcal{G} = (\mathcal{V}_{th} - \mathcal{V}_r)g \quad (\text{B4})$$

where $\mathcal{V}_r = -60$ mV, $\mathcal{V}_{th} = -50$ mV [61, 62]. Typical values of the parameters employed in this paper were $a = 1.3$, $g = 0.4$, $\alpha = 9$ and they correspond to $\mathcal{R}_{in}J^b = -47$ mV, $\mathcal{G} = 4$ mV, $\tilde{\alpha} = 225$ Hz. For these choices of parameters the average firing rate of the single neurons in the non plastic network was $\simeq 29$ Hz, while it decreased to $\simeq 23$ Hz in presence of STDP plasticity.

As far as the STDP parameters are concerned, from the data reported by Bi & Poo in [15] it emerges that the synaptic strengths of hippocampal glutamatergic neurons are potentiated (depressed) of $\simeq 110\%$ ($\simeq 40\%$) by considering 60 consecutive pairs of pre- and post-synaptic spikes. This amounts to have potentiation (depression) amplitude $p \simeq 0.016$ ($d \simeq 0.0066$) in the model employed to mimic STDP (see Eq. (7)), therefore we can safely affirm that our choices were consistent with the experimental data. The widths of the learning time windows are $\tilde{\tau}_+ = 4$ ms and $\tilde{\tau}_- = 12$ ms. These values are comparable with the rise/decay time of the excitatory post-synaptic potentials $1/\tilde{\alpha} = 4.44$ ms, but definitely smaller than those measured in the experiments, namely $\tilde{\tau}_+ \simeq 13 - 19$ ms and $\tilde{\tau}_- \simeq 34$ ms [15, 18].